A Statistics-Guided Approach to Precise Characterization of Nanowire Morphology

Fei Wang,[†,§] Youngdeok Hwang,[‡,§] Peter Z. G. Qian,[‡,*] and Xudong Wang[†,*]

[†]Department of Materials Science and Engineering and [‡]Department of Statistics, University of Wisconsin—Madison, Madison, Wisconsin 53706. [§]These authors contributed equally to this work.

ABSTRACT Precise control of nanomaterial morphology is critical to the development of advanced nanodevices with various functionalities. In this paper, we developed an efficient and effective statistics-guided approach to accurately characterizing the lengths, diameters, orientations, and densities of nanowires. Our approach has been successfully tested on a zinc oxide nanowire sample grown by hydrothermal methods. This approach has three key components. First, we introduced a novel geometric model to recover the true lengths and orientations of nanowires from their projective scanning electron microscope images, where a statistical resampling method is used to mitigate the practical difficulty of relocating the same sets of nanowires at multiple projecting angles. Second, we developed a sequential uniform sampling method for efficiently acquiring representative samples in characterizing diameters and growing density. Third, we proposed a statistical imputation method to incorporate the uncertainty in the determination of nanowire diameters arising from nonspherical cross-section spinning. This approach enables precise characterization of several fundamental aspects of nanowire morphology, which served as an excellent example to overcome nanoscale characterization challenges by using novel statistical means. It might open new opportunities in advancing nanotechnology and might also lead to the standardization of nanocharacterization in many aspects.

KEYWORDS: nanowire · morphology characterization · statistical methods · sequential sampling

During the last few decades, numerous nanostructures have been discovered and can now be rationally synthesized. Among them, one-dimensional (1D) nanostructures, represented by nanowires (NWs), nanotubes, and nanobelts,[1] are considered as advanced fundamental building blocks for the next generation devices and systems in electronics,[2] optics,[3] sustainable energy,[4] biomedicine,[5] and defense technology.[6] Nowadays, understanding of the formation mechanisms of most nanostructures has been primarily established. The morphology, dimension, and crystallography of those nanostructures can be rationally controlled in the laboratory, which provides a reliable supply of the building blocks. As a result, the cutting-edge research on nanotechnology is gradually shifting from nanomaterial synthesis toward property improvement and nanodevice development. For example, prototypical sensors,[7] solar cells,[8] nanogenerators,[9] light-emitting diodes (LEDs),[10] lasers,[11] and biomarkers[12] have all been demonstrated using 1D nanostructures. They are promising candidates for replacing current technology with advanced performance and novel functionalities. The development of such nanodevices requires precise control and high uniformity of the morphology and properties of the nanostructure building blocks. Length, diameter, and orientation are very basic and very important characteristics of a NW, which directly determine its electrical and optical properties and the performance of the corresponding nanodevices. Although they need to be measured every time when they are made and/or used, the results may vary from one to another due to different tools and methodologies that are used and large deviations can always be found. In the nanometer scale, a small difference in measurement may bring about significant variation in the performance and impair the device reproducibility. To establish a completely reproducible research platform for researchers across different disciplines, a standard methodology for precisely characterizing those properties is greatly desired. Such a methodology will even be required for mass production and quality control for future possible commercialization of nanodevice products. Nonetheless, to establish such a methodology that can provide a simple, accurate, and reproducible characterization demands more than just microscopic analysis. In this paper, we use novel statistical ideas and means to establish a statistics-guided approach to precise characterization of nanowires. Recently, various statistical methods have been successfully used to tackle challenging problems in nanotechnology that are difficult to solve by

*Address correspondence to peterq@stat.wisc.edu, xudong@engr.wisc.edu.

Received for review October 30, 2009 and accepted January 19, 2010.

Published online January 26, 2010. 10.1021/nn901530e

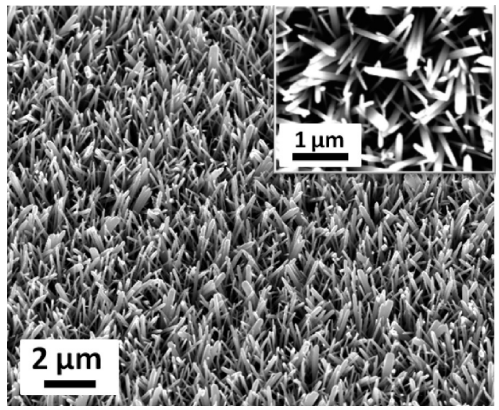

Figure 1. SEM image of a typical ZnO NW array when the sample was tilted by 30°. Inset is a top view image of the NW array.

physical approaches.[13−17] This paper makes further progress in this direction. Our approach addresses three key issues: (a) precisely characterizing the length, orientation, size, and density of a NW forest, which is a typical configuration of most nanowire products; (b) efficiently measuring the general property of the entire NW sample; and (c) unveiling the true information of NWs based on measurements contaminated by external sources of variation in the nanometer scale.

RESULTS AND DISCUSSION

Determination of Nanowire Length. In this section, we consider the important task of estimation of nanowire length. Since a substrate usually contains a large population of nanowires, the objective here is to study the distribution of nanowire length. Statistically, such a distribution can be characterized by the average and spread, that is, the mean and standard deviation (SD). Scanning electron microscopy (SEM) is a popular method for measuring NW length and other morphology. This method is easy to use and provides general information over a large quantity. Other related techniques include transmission electron microscopy (TEM) and scanning probe microscopy (SPM). Currently, details are lacking on how to recover the true morphological characteristics from SEM images. In general, an array of NWs grown on a solid substrate are not exactly vertically aligned or oriented toward the same direction and do not have the same length. For illustration, Figure 1 presents an SEM image of a zinc oxide (ZnO) NW forest grown on a silicon substrate, taken at a tilting angle of 30°. All of the NWs in this figure are grown upward, but not perfectly perpendicular to the substrate. In the top view SEM image (inset of Figure 1), the NWs tilt at different angles. This figure indicates that the projective lengths of NWs measured from SEM images are different from their true lengths. In addition, for a given SEM imaging angle, the variation in the orientation of NWs leads to uncertainty in the projecting angles, which rules out the possibility of determining the length distribution of NWs from a single SEM image. To mitigate this difficulty, we introduced a three-dimensional geometric model, coupled with a statistical estimation method to recover the true length distribution of NWs from the projections of the lengths of the NWs measured from SEM images. This method can precisely determine the length distribution and the orientation distribution of NWs.

The geometric model is presented in Figure 2a, where the solid blue line (*OA*) represents a NW grown on a solid substrate on the $x-y$ plane. Let K denote the length of the NW in Figure 2a. In terms of statistical terminology, K is a random variable, and hence the objective here is to estimate the expected value of K, denoted by $E(K)$, and the variance of K, denoted by var(K). In Figure 2a, the orientation of the NW is defined in terms of the angle α, which captures how the NW is vertically aligned on the substrate. In the figure, γ denotes the angle between the NW and the $y-z$ plane and δ the angle between the $+y$ axis and the projection of the NW onto the $y-z$ plane, given by the dotted blue line (OA'). The projection of the NW on the SEM image is the dashed blue line (*OB*) with length L. From this geometric model, it can be verified that

$$A'B' = OA' \times \sin(180^\circ - \delta) = OA \times \cos\gamma \times \sin\delta \tag{1}$$

where $A'B'$ is the projection of the NW onto the z axis with length $(K^2 - L^2)^{1/2}$. We have

$$\sqrt{K^2 - L^2} = K \times \cos\gamma \times \sin\delta \tag{2}$$

and α can be expressed as

$$\sin\alpha = \frac{\sqrt{K^2 - L^2}}{K} \tag{3}$$

Combining eqs 2 and 3

$$\alpha = \sin^{-1}(\cos\gamma \times \sin\delta) \tag{4}$$

where $\alpha = 90°$ means that the NW is exactly perpendicular to the substrate.

Because three independent equations are required for solving for the three unknowns, K, γ, and δ, in eq 2, the NW samples are tilted at three different angles θ_1, θ_2, and θ_3, and at each θ_i, the projected NW length L_i is measured from the SEM image. As shown in Figure 2b, when the NW sample is tilted around the x axis by an angle θ, angle δ becomes $(\delta - \theta)$ and all the other parameters remain unchanged. Similarly, from eq 2, we have

$$\begin{cases} \sqrt{K^2 - L_1^2} = K \times \cos\gamma \times \sin(\delta - \theta_1) \\ \sqrt{K^2 - L_2^2} = K \times \cos\gamma \times \sin(\delta - \theta_2) \\ \sqrt{K^2 - L_3^2} = K \times \cos\gamma \times \sin(\delta - \theta_3) \end{cases} \tag{5}$$

The values of K, γ, and δ can be determined by solving eq 5 and consequently α can be obtained from eq 4.

Following the developed method described above, we measured the projective lengths of the NW array in our experiment at $\theta_1 = 15°$, $\theta_2 = 30°$, and $\theta_3 = 45°$ to recover the distributions of the true length and orientation of the NWs. In general, for a NW array with high density, a random cleavage of the NW sample should be taken to represent the general property of the NW array. Also, to measure the projective length of a NW at a tilting angle, its root and top should be observable. For illustration, Figure 2c shows cleavage of a NW sample, where the NWs with observable roots and tips are marked by the blue lines. In our experiment, measurements were conducted at random locations from the NW sample, and at each θ_i, the projective lengths L_i of about 30−40 NWs with observable roots and tips were measured. The mean and SD of the L_1, L_2, and L_3 values are given in Table 1. Figure 3 is the Box−Whisker plot[18] of the L_1, L_2, and L_3 data, where each black dot indicates one projective NW length. The upper and lower borders of the box in the figure represent the largest 25% and smallest 25% of the observations, respectively. The middle gray bar inside the box, representing the sample median, divides the data into two halves. The data points outside the gray lines are classified as outliers.

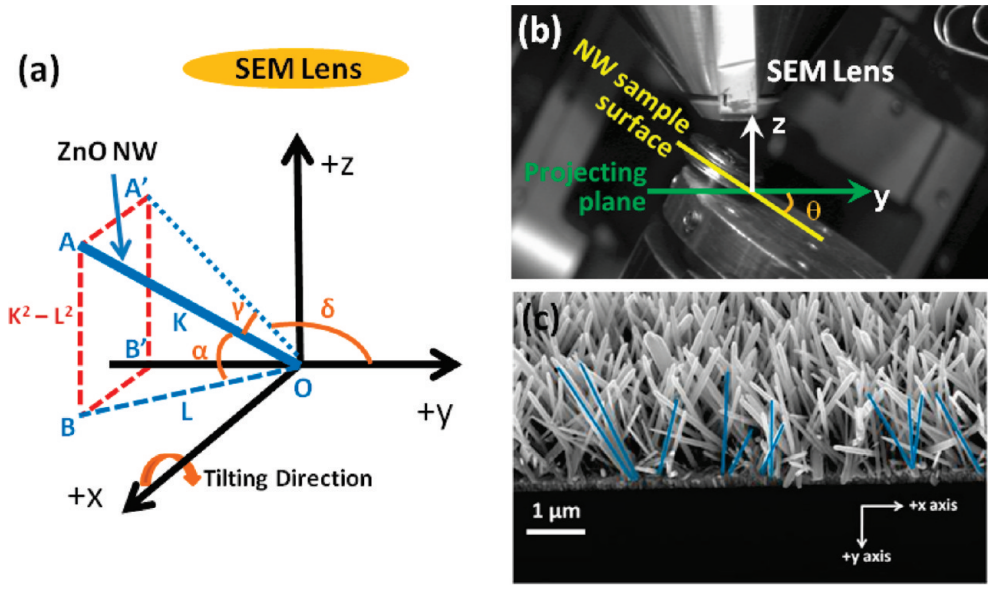

Figure 2. (a) Schematic illustration of the geometric model used to recover the true length of a ZnO NW. (b) Optical image of LEO 1530 SEM chamber revealing the tilting situation of SEM imaging. (c) One SEM image of ZnO NWs on the edge of a piece of silicon wafer for length and orientation measurements. The sample was tilted by 45°.

Note that eq 5 requires projective lengths of the same NWs at different tilting angles to recover the true length K. This is, however, impractical due to the mismatching between the nanoscale imaging and macroscale sample rotating. To overcome this obstacle, we developed a novel statistical method for estimating the true length of NWs without measuring lengths from the same NWs in all three angles. The method consists of three steps. (1) For each θ_i, randomly divide the observations into m mutually exclusive subsets and let L_{ij} denote the average of the L_i values of the jth subset. (2) For $j = 1, ..., m$, let K_j and α_j be K and α obtained by plugging L_{1j}, L_{2j}, and L_{3j} into eqs 4 and 5. (3) Use the sample mean and sample variance of K_j values to estimate the mean and variance of K, and use the sample mean and sample variance of α_j values to estimate the mean and variance of α.

For situations in which the measurements are sorted in some certain order, it is recommended to randomly permute the data before performing the division in step 1. The developed method can be easily implemented in computer languages like R and Matlab. In our experiment, we applied the developed method to divide the data into $m = 5$ subsets and obtained the estimated mean of K to be 2117 nm with SD 916 nm and the mean

TABLE 1. Means and SDs of the L_1, L_2, and L_3 Values Measured from SEM Images at $\theta_1 = 15°$, $\theta_2 = 30°$, and $\theta_3 = 45°$

tilting angle	$\theta_1 = 15°$	$\theta_1 = 15°$	$\theta_1 = 15°$
mean (nm)	1013	1253	1493
SD (nm)	437	565	577

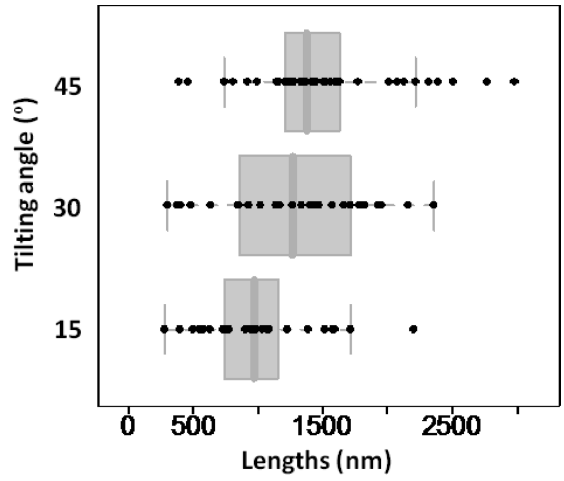

Figure 3. Raw data of the measured length of NWs. Each measurement is drawn as a black dot, while the box plot represents a reference for the dispersion. Upper and lower borders of the box indicate the first and third quartiles, and the middle bar on the box is the median. The points exceeding the gray bars are classified as outliers.

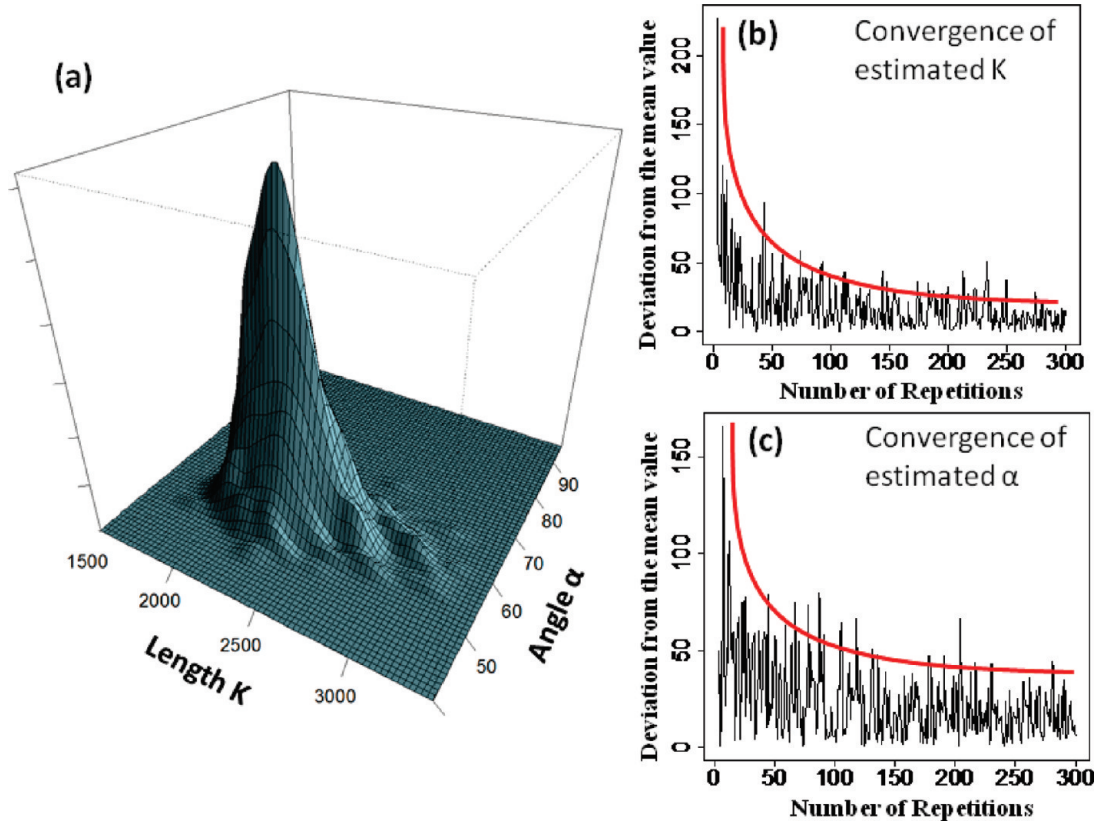

Figure 4. (a) Distribution of the recovered length and orientation of NWs. The mean of *K* was estimated at 1933 nm with SD of 507 and the mean of α was estimated to be 59 with SD of 8. (b) Convergence of the estimated of the mean of *K*. (c) Convergence of the estimated mean of α.

of α to be 57° with SD 17°. It is possible to obtain the sampling distribution of the estimators from the developed method by repeatedly dividing the data in step 1. For illustration, Figure 4a presents the density of the means of *K* and α given by repeatedly applying the procedure 100 times to the data of our experiment. Let *K** and α* denote the means of *K* and α computed by applying the procedure 400 times. Figure 4b plots the deviation of the mean of *K* from *K** for our experiment against the number of times the data were divided in step 1, and Figure 4c plots the deviation of the mean of α from α* for our experiment against the number of times the data were divided in step 1. These figures indicate that the means of *K* and α become stable when the procedure is repeated 150 times.

Determination of Nanowire Density. The density of a NW array is usually defined to be the number of NWs located per unit area. The density is another fundamental property of NW arrays that affects the overall performance of NW-based devices. For example, NW density determines the roughness factor that is directly related to the efficiency of solar energy conversion,[8] the catalytic ability,[19] or the capacitance of charge or molecules.[20,21]

It is always contradictory when a macroscale general property is needed to be determined on nanoscale samples. In order to be accurate and representative, one needs to perform the measurement on as many individual samples as possible. On the other hand, the nanoscale feature of the targeting sample restricts the measurements into a very small area. The density measurement is such a case. NWs can only be counted within a very small area each time. However, the density in a tiny area may not fully represent the density of the entire sample due to the density fluctuations in the small scale (*e.g.*, micrometers in our ZnO sample). As a result, how to decide the data sampling area becomes critical.

Besides, as in many other scientific experiments, it is important to balance the accuracy and the resources provided in the experiment. One is often interested in obtaining information about the NWs as much as possible with minimum experimental efforts.[18] Therefore, for taking measurements of the NWs, an efficient strategy that balances the amount of information and the available resources is highly desired to decide how many and which nanowires should be measured. It is also beneficial if measurements can be taken in a sequential manner.[22] Here we propose a two-stage procedure for uniformly measuring the NW density. The basic idea is to take measurements from selected areas with two levels of fineness. The imaging area is divided into equally spaced big $n_1 \times n_1$ cells by a coarse grid (labeled as I, II, ..., n_1) and in the meantime into $n_2 \times n_2$ equally spaced small cells (labeled as 1, 2, ..., n_2), where n_1 and n_2 are positive integers where n_2 is a multiple of

n_1. Figure 5 illustrates such a plan with $n_1 = 4$ and $n_2 = 8$. On the basis of the two types of cells, the procedure consists of two steps. (1) Randomly pick n_1 cells from the n_1^2 small cells such that each column and each row of the imaging area contain precisely one cell. Then from each chosen large cell, randomly pick one small cell inside the large cell to perform measurement. (2) Among the $n_2 - n_1$ rows and $n_2 - n_1$ columns in which no cells were chosen in step 1, randomly pick $n_2 - n_1$ additional small cells such that after combined with the cells chosen in stage 1, each row and each column of the fine grid has one and exactly one small cell to be chosen.

Estimates associated with this scheme will have smaller variances than their counterparts chosen by using simple Monte Carlo sampling. Using a ZnO NW array shown in Figure 5 for illustration, the coarse and fine grid layers had 16 and 64 unit cells, respectively, with $n_1 = 4$ and $n_2 = 8$. In the first step, the cells labeled by (I, II), (II, I), (III, III), and (IV, IV) were chosen, indicated by green color. The small unit cells chosen among the green ones were in yellow. The four additional cells chosen in stage 2 were in gray. Combining four yellow cells and four gray cells gave eight cells that were distributed uniformly in the substrate; each row and column contain precisely one cell. The numbers of NWs located in these eight cells will then be used to determine the NW's density.

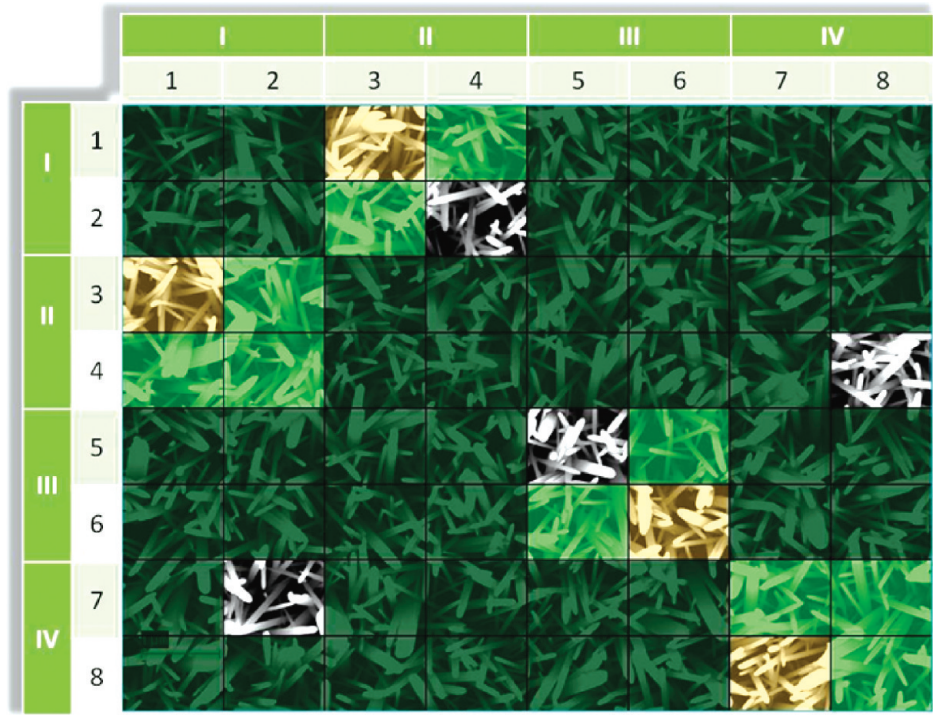

Figure 5. Sequential procedure for determining the density of NWs. The yellow-shaded cells are the four cells that were chosen in the first step. If the space is divided by a 4 × 4 matrix (marked by Roman numbers), these four cells take up every row and column. The four transparent cells are what were chosen in the second stage. The total eight cells also take up every row and column of the 8 × 8 matrix.

An additional set of data was collected following the same procedure from another SEM image that was taken at a different location of the substrate. The results from these two locations are summarized in Table 2. The overall average was 21.2 NWs per cell. Because the area of one cell was 2.40 μm^2, the density of the NW sample was 8.83×10^5 NW/cm^2. If only the first step was done on location 1, the result would be 22.25 NWs per cell, which gives the density of 9.27×10^5 NW/cm^2. The difference between numbers received from the two stages is about 5%, which can be considered as generic variation among the NWs due to the small number of observations. Depending on the requirement of accuracy in different cases, one may move on to the second step, which will give a more precise result.

The above method presented a novel scheme for measuring the data in one image and can produce estimators with smaller variance than those from simple Monte Carlo sampling. Variance formulas of this scheme can be found by using some combinational methods.[22] In order to retrieve representative information of the entire NW sample, more observing areas should be included. Distribution of the observing areas can also be arranged and selected based on the same sequential method. In general, this method is particularly useful for nanocharacterization sampling when the features of interests do not distribute evenly across the sample area.

Determination of Nanowire Diameter. Diameter is yet another fundamental parameter of the NW morphology, widely considered as a primary measure for evaluating the sample uniformity. The NW diameters are typically measured by SEM, or by TEM when the diameter of the

TABLE 2. Summary of the Numbers of Nanowires in Each Cell That We Have Chosen to Count

		step 1				step 2			
		cell 1	cell 2	cell 3	cell 4	cell 1	cell 2	cell 3	cell 4
location 1	# NWs	20	22	24	23	25	18	18	20
	average		22.25						
	average						21.25		
location 2	# NWs	19	22	15	20	17	27	22	27
	average		19.00						
	average						21.12		
overall average					21.18				

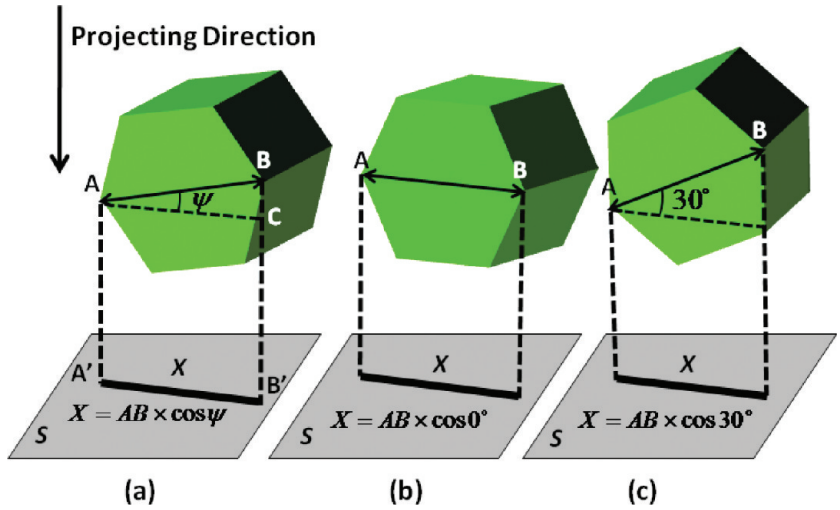

Figure 6. Illustration of the relationship between the true diameter of a NW and its projective diameter.

NW is too small to be imaged sharply under SEM. Here, we discuss a method for the case of SEM imaging, which can be directly applied to TEM or even SPM imaging because both of them can also be considered as a 2D projection of 3D features. In an SEM image, the projected thickness is independent of the NW's orientation angle, given as α in Figure 2a. However, one artifact that should be considered is the shape of the NW's cross section, which might distort the actual diameter of a NW. For example, the projected thickness of a NW with a hexagonal cross section depends on the spinning angle of the NW, denoted by ψ. As shown in Figure 6a, ψ is the angle between the NW's longest diagonal, *AB*, and the horizontal line, *AC*, which is parallel to the projecting plane, *S*. The diameter of such a hexagonal NW is defined as the length of *AB*. On a projective image, the observed diameter, denoted by *X*, is distorted by the spinning angle in the following manner:

$$X = AB \times \cos\psi \qquad (6)$$

From eq 6, the maximum value of *X* is the *AB*, where $\psi = 0°$, as shown in Figure 6b. However, the majority of *X* would be observed to be smaller than *AB*, where the smallest value is observed when $\psi = 30°$, as shown in Figure 6c. Due to the six-fold symmetry of the NW's cross section, all possible measurements fall into the range of $0° \leq \psi \leq 30°$. As a result, even for an array of NWs with the same diameter, the variation of the spinning angle ψ can give rise to variation to the observed *X* values. The variation could be as large as 13.4% of the actual diameter. Thus, if the diameters were directly determined from the projected image, the mean and SD would always be biased. It should be noted that this problem exists in all noncylindrical-shaped NWs, including triangular, rectangular, *etc*. In view of this problem, we developed a statistical method for recovering the true mean and SD of *AB* values using the observed *X* values.

The main idea is to adjust the angle ψ using a statistical imputation procedure.[23] For clarity, let subscript *i* denote the projected diameter, spinning angle, and true diameter corresponding to the *i*th observation. For example, the values of the first observation are denoted X_1, ψ_1, and AB_1. It is reasonable to assume that the ψ_i values are uniformly distributed on [0°, 30°], independent of the diameter AB_i. First, using the random number generator in R 2.8.1,[24] a random sequence of angles that are uniformly distributed between 0 and 30° is generated. This can also be done in Excel by using the function RAND. The number of angles in this random sequence is the same as that of observations. The randomly generated ψ_i works as the true ψ_i and can be used to recover the AB_i using eq 6. Then, a simulated $\bar{A}\bar{B}_i$ is obtained by dividing X_i and find the mean and SD of all $\bar{A}\bar{B}_i$ values. This procedure should be repeated a number of times to obtain multiple simulated means and SDs, the averages of which will reveal the mean and SD of the true diameter, AB_i.

For our ZnO NW sample, we measured the diameters of NWs from the 32 unit cells chosen by the sequential procedure introduced during NW density determination with $n_1 = 16$ and $n_2 = 32$. To measure the diameters of a reasonable number of NWs, an SEM image was divided into 1024 unit cells by a 32×32 matrix. Thirty-two unit cells are chosen out of a 32×32 matrix, within which the NWs were measured. The above imputation method gave the mean diameter of 97 nm with SD of 33 nm, whereas the mean and SD directly calculated from the observed diameter were 92 and 31 nm, respectively. The estimated mean diameter using the imputation method was larger than the mean of the observed. The two SDs also differed slightly but did not differ in terms of relative standard deviation (RSD). The RSD of *X* values was $33/97 \approx 34.02\%$ and that of simulated *AB* values was $31/92 \approx 33.7\%$. Figure 7 indicates that when the developed method is applied to our example the estimated mean *AB* converges when the number of repetitions reaches 200.

With slight modification, the developed approach is also applicable to NWs with other types of cross sections, such as triangular or rectangular shapes, where eq 6 needs to be changed according to the relationship between the true diameter and projective diameter. The sequences of projecting angles can be generated

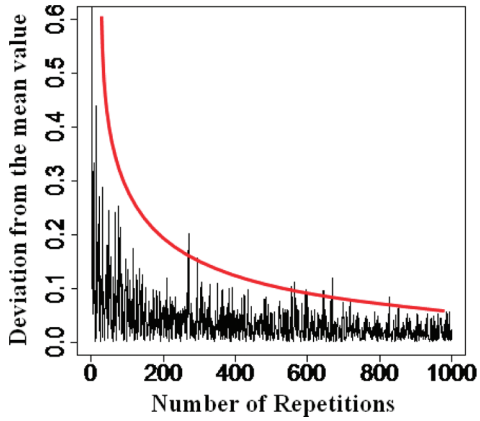

Figure 7. Convergence of the estimated mean diameter, *AB* values. Reference line is drawn to show the convergence of the estimated value.

either randomly or with preferences in a case by case manner.

CONCLUSIONS

In this paper, we developed a statistical approach for precisely characterizing the lengths, diameters, orientations, and density of NWs. This method was illustrated using ZnO NW arrays grown by hydrothermal methods. For length and orientation characterization, we developed a geometric model, coupled with the resampling idea in statistics, to recover the true lengths and orientation of NWs from their projective images observed under SEM. For characterizing diameters and density, we introduced a sequential uniform sampling method to efficiently acquire representative data while giving the flexibility to trade off between experimental efforts and accuracy. We also introduced an imputation method to incorporate the uncertainty in diameter determination rising from nonspherical cross-section spinning. This work presents a precise quantitative characterization of several key aspects of NW morphology, which would further feedback on synthesis optimization and scaling-up in a more repeatable and efficient manner. This research presented an excellent example to overcome nanoscale characterization challenges by integrating nanotechnology with novel statistical methods. Such approaches might open new opportunities in advancing nanotechnology and might also lead to the standardization of nanocharacterization in many aspects.

EXPERIMENT

For the growth of the zinc oxide nanowire array on silicon substrate, a thin layer of zinc oxide was first deposited as nucleation seeds. To do this, a few drops of 5 mM zinc acetate ethanol solution were dipped on the silicon substrate and blown dry. Subsequent to repeating this dip-coating three times, the substrate was placed in an oven and baked at 350 °C for 20 min. The seed-coated substrate was placed in a vial, facing down on the surface of the solution containing 25 mM zinc nitrate, 25 mM hexamethylenetetramine, and 2 g/L branched polyethylenimine. The reaction was performed at 90 °C for up to a day. SEM images were taken using LEO 1530, and length measurements were made by image processing software Image Pro based on SEM images.

The statistical methods developed in this paper were implemented using R 2.8.1,[24] a free statistical computing environment, which can also be implemented by using Microsoft Excel.[25] Some developed R programs are available from the authors.

Acknowledgment. This work was supported by the National Science Foundation under Grant Nos. CMMI-0926245 and DMS-0705206 and a faculty award from IBM.

REFERENCES AND NOTES

1. Xia, Y. N.; Yang, P. D.; Sun, Y. G.; Wu, Y. Y.; Mayers, B.; Gates, B.; Yin, Y. D.; Kim, F.; Yan, Y. Q. One-Dimensional Nanostructures: Synthesis, Characterization, and Applications. *Adv. Mater.* **2003**, *15*, 353–389.
2. Cui, Y.; Lieber, C. M. Functional Nanoscale Electronic Devices Assembled Using Silicon Nanowire Building Blocks. *Science* **2001**, *291*, 851–853.
3. Law, M.; Sirbuly, D. J.; Johnson, J. C.; Goldberger, J.; Saykally, R. J.; Yang, P. D. Nanoribbon Waveguides for Subwavelength Photonics Integration. *Science* **2004**, *305*, 1269–1273.
4. Tian, B. Z.; Zheng, X. L.; Kempa, T. J.; Fang, Y.; Yu, N. F.; Yu, G. H.; Huang, J. L.; Lieber, C. M. Coaxial Silicon Nanowires as Solar Cells and Nanoelectronic Power Sources. *Nature* **2007**, *449*, 885-U8.
5. Kam, N. W. S.; Dai, H. J. Carbon Nanotubes as Intracellular Protein Transporters: Generality and Biological Functionality. *J. Am. Chem. Soc.* **2005**, *127*, 6021–6026.
6. Wang, Z. L. Towards Self-Powered Nanosystems: From Nanogenerators to Nanopiezotronics. *Adv. Funct. Mater.* **2008**, *18*, 3553–3567.
7. Wan, Q.; Li, Q. H.; Chen, Y. J.; Wang, T. H.; He, X. L.; Li, J. P.; Lin, C. L. Fabrication and Ethanol Sensing Characteristics of ZnO Nanowire Gas Sensors. *Appl. Phys. Lett.* **2004**, *84*, 3654–3656.
8. Law, M.; Greene, L. E.; Johnson, J. C.; Saykally, R.; Yang, P. D. Nanowire Dye-Sensitized Solar Cells. *Nat. Mater.* **2005**, *4*, 455–459.
9. Wang, X. D.; Song, J. H.; Liu, J.; Wang, Z. L. Direct-Current Nanogenerator Driven by Ultrasonic Waves. *Science* **2007**, *316*, 102–105.
10. Qian, F.; Gradecak, S.; Li, Y.; Wen, C. Y.; Lieber, C. M. Core/Multishell Nanowire Heterostructures as Multicolor, High-Efficiency Light-Emitting Diodes. *Nano Lett.* **2005**, *5*, 2287–2291.
11. Johnson, J. C.; Yan, H. Q.; Yang, P. D.; Saykally, R. J. Optical Cavity Effects in ZnO Nanowire Lasers and Waveguides. *J. Phys. Chem. B* **2003**, *107*, 8816–8828.
12. Zheng, G. F.; Patolsky, F.; Cui, Y.; Wang, W. U.; Lieber, C. M. Multiplexed Electrical Detection of Cancer Markers with Nanowire Sensor Arrays. *Nat. Biotechnol.* **2005**, *23*, 1294–1301.
13. Casella, G. R., L.; Berger, R. L. *Statistical Inference*; Duxbury Press: Pacific Grove, CA, 2001.
14. Dasgupta, T.; Ma, C.; Joseph, V. R.; Wang, Z. L.; Wu, C. F. J. Statistical Modeling and Analysis for Robust Synthesis of Nanostructures. *J. Am. Stat. Assoc.* **2008**, *103*, 594–603.
15. Deng, X. W.; Joseph, V. R.; Mai, W. J.; Wang, Z. L.; Wu, C. F. J. Statistical Approach To Quantifying the Elastic Deformation of Nanomaterials. *Proc. Natl. Acad. Sci. U.S.A.* **2009**, *106*, 11845–11850.
16. Dasgupta, J. T.; Wu, C. F. J. Minimum-Energy Designs: from Nanostructure Synthesis to Sequential Optimization. Submitted for publication.

17. Xu, S.; Adiga, N.; Ba, S.; Dasgupta, T.; Wu, C. F. J.; Wang, Z. L. Optimizing and Improving the Growth Quality of ZnO Nanowire Arrays Guided by Statistical Design of Experiments. *ACS Nano* **2009**, *3*, 1803–1812.
18. Wu, C.-F.; Hamada, H. *Experiment: Planning, Analysis, and Parameter Design Optimization*; Wiley: New York, 2009.
19. Kolmakov, A.; Klenov, D. O.; Lilach, Y.; Stemmer, S.; Moskovits, M. Enhanced Gas Sensing by Individual SnO_2 Nanowires and Nanobelts Functionalized with Pd Catalyst Particles. *Nano Lett.* **2005**, *5*, 667–673.
20. Wang, X. D.; Zhou, J.; Lao, C. S.; Song, J. H.; Xu, N. S.; Wang, Z. L. *In Situ* Field Emission of Density-Controlled ZnO Nanowire Arrays. *Adv. Mater.* **2007**, *19*, 1627.
21. Wang, X. D.; Song, J. H.; Summers, C. J.; Ryou, J. H.; Li, P.; Dupuis, R. D.; Wang, Z. L. Density-Controlled Growth of Aligned ZnO Nanowires Sharing a Common Contact: A Simple, Low-Cost, and Mask-Free Technique for Large-Scale Applications. *J. Phys. Chem. B* **2006**, *110*, 7720–7724.
22. Qian, P. Z. G. Nested Latin Hypercube Designs. *Biometrika* **2009**, *96*, 957–970.
23. Hastie, T.; Ribshirani, R.; Friedman, J. *The Elements of Statistical Learning: The Elements of Statistical Learning*; Springer-Verlag: Berlin, 2000.
24. Hornik, K. *The R FAQ*; http://CRAN.R-project.org/doc/FAQ/R-FAQ.html; ISBN 3-900051-08-9.
25. Walkenbach, J. *Excel 2007 Bible*; Wiley: New York, 2007.